

# Coulomb potential screening via charged carriers and charge-neutral dipoles/excitons in two-dimensional case

Ke Xiao<sup>1,2\*</sup>, Chiming Kan<sup>1,3\*</sup>, Xiaodong Cui<sup>1</sup>

<sup>1</sup> Department of Physics, University of Hong Kong, Hong Kong SAR

<sup>2</sup> NISE Department, Max Planck Institute of Microstructure Physics, Halle, Germany

<sup>3</sup> Department of Chemistry, Hong Kong University of Science and Technology, Hong Kong SAR

\* Email: [Ke.Xiao@mpi-halle.mpg.de](mailto:Ke.Xiao@mpi-halle.mpg.de) and [cmkanaa@connect.ust.hk](mailto:cmkanaa@connect.ust.hk)

## Abstract:

With the shrink of dimensionality, Coulomb interaction displays a distinct role owing to the reduced dielectric screening in out-of-plane direction. Apart from the dielectric screening, the free charge carriers and/or dipoles can also make nonnegligible contribution to Coulomb interaction. While the Thomas Fermi model is effective in describing charge carrier screening in three dimensions, the extent of screening to two-dimension resulting from charge-neutral dipoles and carriers remains quantitatively unclear. To address this gap, we present a simple analytical solution based on linear response theory, offering a comprehensive depiction of the Coulomb screened potential in both 2D and 3D systems, where screening effects from both charge carriers and charge-neutral dipoles are addressed. Our work provides a handy tool for directly analysing and evaluating Coulomb interaction strength in atomically thin materials and particularly in the context of electronic and optoelectronic engineering. As a demonstration, we utilize the derived modified Coulomb potential for the exciton system to estimate the exciton binding energy variation arising from exciton density fluctuation and the temperature dependent exciton polarizability, yielding excellent agreement with the experimental and computational findings.

## Introduction:

The rise of atomically thin two-dimensional (2D) materials provides an ultimate 2D platform for physics research and great promise of applications from their fascinating properties. With the shrink of dimensionality, Coulomb interaction is greatly enhanced owing to reduced dielectric screening and spatial confinement.<sup>1,2</sup> This enhanced Coulomb interaction plays a more significant role in electronic properties of the 2D materials than their three-dimension (3D) counterparts, usually determining characteristic optical and electric properties of 2D materials. Renowned evidences include the giant exciton binding energy,<sup>3-5</sup> the significant renormalization of electronic bandgap<sup>6,7</sup>, moiré excitons in 2D heterostructures<sup>8-10</sup>, enhanced superconductivity<sup>11,12</sup> etc. It is one of the concurrently focused topics to elaborate Coulomb interactions in depicting exotic phenomena in 2D materials.<sup>13-15</sup>

In contrast to 3D cases where the macroscopic Coulomb screening is well described by a

single macroscopic dielectric constant  $\epsilon_r$ , more accurately a permittivity tensor in the modified Coulomb potential (Fig. 1(a)), the macroscopic screening in 2D dielectric cases is highly nonlocal<sup>16-18</sup> and the induced polarization is confined to the 2D plane (Fig. 1(b)), resulting in a suppression of dielectric screening in the out-of-plane direction. The Coulomb potential due to this contrasting polarization in 2D is widely described in Rytova-Keldysh form<sup>19</sup>,  $V_{2D}(r, z = 0) = -\frac{e^2}{8\epsilon_0 r_0} \left[ H_0\left(\frac{\epsilon_r r}{r_0}\right) - Y_0\left(\frac{\epsilon_r r}{r_0}\right) \right]$ . It displays a logarithmic divergence ( $V_{2D}^{app} = \frac{e}{4\pi\epsilon_0} \left[ \ln\left(\frac{\epsilon_r r}{r_0}\right) + \gamma \right]$ ) at a short-separation limit and reduces to the conventional 3D screened potential ( $V_{3D} = \frac{e}{4\pi\epsilon_r\epsilon_0 r}$ ) at long-range (Fig. 1(c)). Apart from the polarization from periodical crystal lattice, when charge carriers and electric dipoles exist, the Coulomb potential is further screened. Typically, in a 3D system, screened Coulomb potential arising from charge carriers is well described by the Thomas-Fermi model or Lindhard theory<sup>20</sup>. An exponential damping term is exerted to the long-ranged Coulomb potential, making it short-ranged. When it comes to the 2D system, although electrostatic doping has been extensively studied in different kinds of 2D materials<sup>21-29</sup>, the interplay of bandgap renormalization<sup>30-32</sup> and polaron effect<sup>31,33</sup> makes it difficult to resolve the screening effect experimentally. Beside the contribution from charge carriers, the screening effect from electric dipoles which is usually neglected owing to charge-neutral, could be significant in some scenarios particularly at a modest dipole density.<sup>34,35</sup> Recently, the screening effect of electric dipoles has been experimentally addressed in exciton system of monolayer TMDs<sup>36,37</sup>. It stimulates further investigation on how electric dipoles contribute to screening Coulomb interaction at the microscopic level. A general and specific quantitative description of the screened Coulomb potential arising from charge carriers and charge-neutral dipoles remains unclear.

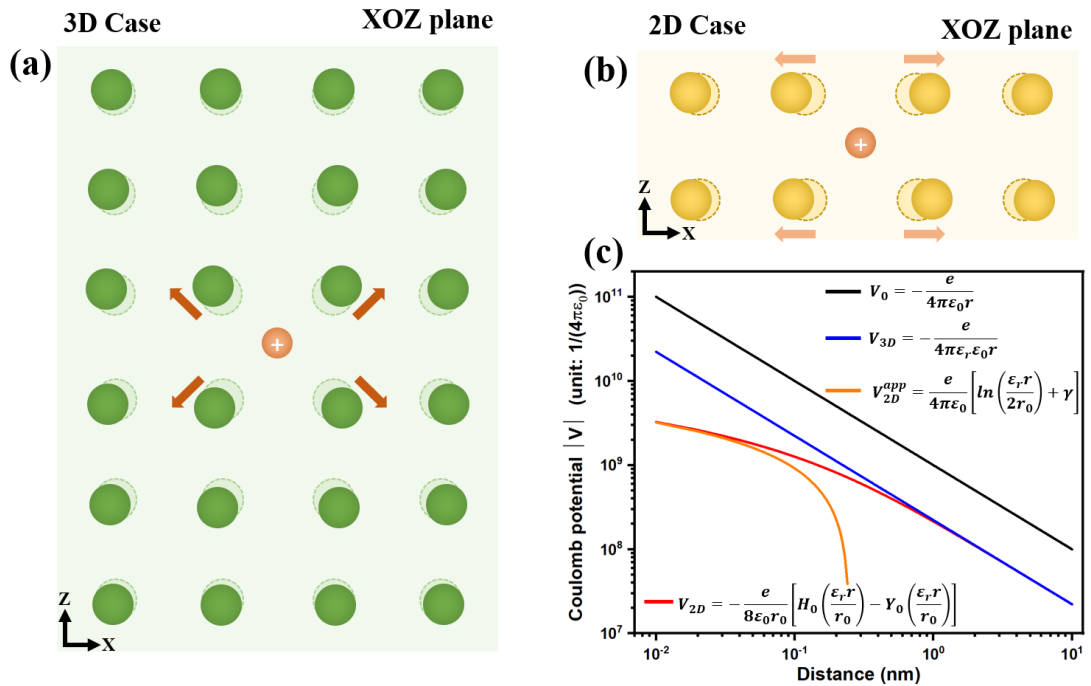


Figure 1: Dielectric polarization in 3D case (a) and 2D case (b). In 2D case, the system is

polarizable inside the 2D plane, leading to a nonlocal macroscopic screening. (c) Coulomb potentials under different screening situations.

This letter presents a simple analytical solution to describe the Coulomb screened potential in both 2D and 3D cases with linear response theory, where screening effects from both charge carriers and charge-neutral dipoles are taken into consideration. Additionally, we cross check with independent perturbation theory, which serves as a strong validation of our approach. Using the derived Coulomb potential, we calculated the exciton binding energy as a function of exciton density and estimated the 2D exciton polarizability, both well aligning with the experimental results. Our work provides a handy tool for analysing and estimating Coulomb interactions strength in atomically thin materials and particularly for engineering design in electronics and optoelectronics applications.

### Derivation of modified Coulomb potential under screening effect from charge carriers and charge-neutral dipoles:

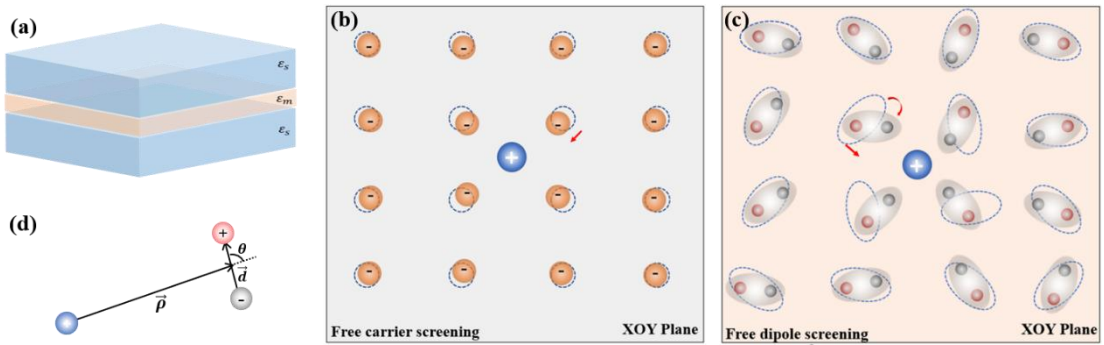


Figure 2: Schematic representation of a dielectric sheet ( $\epsilon_m$ ) encapsulated in a dielectric environment ( $\epsilon_s$ ) (a) and screening effect from charge carriers (b) and charge-neutral dipoles (c). Dipole can contribute to the screening electrostatic potential via dipole shift and rotation.

#### Charge carrier screening:

To incorporate the effect of carrier screening in 2D case, we introduce a dielectric sheet ( $\epsilon_m$ ) with negligible thickness encapsulated in a dielectric environment ( $\epsilon_s$ ) (Fig.2a). Initially, the system is in thermodynamic equilibrium according to the Jellium model with a uniform carrier density ( $n_{carrier}(\rho) = cons.$ )<sup>38</sup>. The system is perturbed with a point charge ( $e\delta(r)$ ) introduced at the origin at time  $t_0$ , described by a time-dependent perturbative term

$$(H_{1,s}(t) = \begin{cases} 0, & t < t_0 \\ V_I(t), & t \geq t_0 \end{cases}).$$

As a result, the carrier density is lifted to an induced carrier

$$\text{density defined as } n_{carrier}^{ind}(\rho, t) = n_{carrier}(\rho, t) - n_{carrier}(\rho, 0).$$

The screened Coulomb potential ( $\varphi(\mathbf{r})$ ) arising from the external point charge at the origin can be described by Poisson's equation:

$$\nabla^2 \varphi(\mathbf{r}) = -\frac{e}{\varepsilon_0} \delta(\mathbf{r}) - \frac{e}{\varepsilon_0} n^{ind}(\mathbf{r}) \quad (1)$$

Here,  $en^{ind}(\mathbf{r})$  represents the induced charge density given by  $en^{ind}(\mathbf{r}) = \alpha_s \nabla^2 \varphi(\mathbf{r}) - \alpha_s^{2D} \nabla_\rho^2 \varphi(\boldsymbol{\rho}, z=0) \delta(z) + \alpha_m^{2D} \nabla_\rho^2 \varphi(\boldsymbol{\rho}, z=0) \delta(z) + en_{carrier}^{ind}(\boldsymbol{\rho}, z=0) \delta(z)$ , where  $\alpha_s$  and  $\alpha_m^{2D}$  represent the polarizabilities of the surroundings and dielectric sheet, which are linked to the macroscopic polarization by  $\mathbf{P}_s = -\alpha_s \nabla \varphi(\mathbf{r})$ ,  $\mathbf{P}_s^{2D} = -\alpha_s^{2D} \nabla_\rho \varphi(\boldsymbol{\rho}, z=0)$ ,  $\mathbf{P}_m^{2D} = -\alpha_m^{2D} \nabla_\rho \varphi(\boldsymbol{\rho}, z=0)$ , respectively. The final term encodes the screening effect from charge carriers.

Under the interaction picture, the dynamics of induced carrier density in 2D case could be written with the linear response theory:

$$n_{carrier}^{ind}(\boldsymbol{\rho}, t) = -\frac{i}{\hbar} \theta(t-t') \int_{-\infty}^{+\infty} dt' \langle [\hat{n}_I(\boldsymbol{\rho}, t), V_I(t')]_- \rangle \quad (2)$$

Where  $\theta(t) = -\lim_{\eta \rightarrow 0^+} \frac{1}{2\pi i} \int_{-\infty}^{+\infty} d\omega \frac{e^{-i\omega t}}{\omega + i\eta}$ , is the Heaviside step function;  $V_I(t') = e\varphi(\boldsymbol{\rho}', t') \hat{n}(\boldsymbol{\rho}', t')$  is the potential energy coupled to the carrier density at time  $t'$ . Conforming to the definition of two-particle Green's function:  $\chi_{carrier}(\boldsymbol{\rho}, \boldsymbol{\rho}'; t, t') = -\frac{i}{\hbar} \theta(t-t') \langle [\hat{n}_I(\boldsymbol{\rho}, t), \hat{n}_I(\boldsymbol{\rho}', t')]_- \rangle$ , the induced carrier density could be further written as:

$$n^{ind}(\boldsymbol{\rho}, t) = e \int_{-\infty}^{+\infty} dt' d^2 \boldsymbol{\rho}' \chi_{carrier}(\boldsymbol{\rho} - \boldsymbol{\rho}'; t-t') \varphi^{ext}(\boldsymbol{\rho}', t') \quad (3)$$

Insert equation (3) into equation (1) and perform Fourier transform (FT) on both sides with the static limit ( $\omega \rightarrow 0$ ) taken:

$$(q^2 + k_z^2) \varphi(\mathbf{q}, k_z) = -\frac{1}{\varepsilon} \left( e + q^2 \frac{\alpha_{total}^{2D}}{2\pi} \int_{-\infty}^{+\infty} \varphi(\mathbf{q}, k_z) dk_z \right) - \frac{e}{\varepsilon} \chi(\mathbf{q}) \int_{-\infty}^{+\infty} \varphi(\mathbf{q}, k_z) dk_z \quad (4)$$

where  $\varepsilon = \varepsilon_0 + \alpha_s$ ,  $\alpha_{total}^{2D} = \alpha_m^{2D} - \alpha_s^{2D}$ . The Fourier transform of  $\chi_{carrier}$  is obtained to be

$$\chi(\mathbf{q}) = \frac{1}{S} \sum_{\mathbf{k}} \frac{(f(\varepsilon_{\mathbf{k}+\mathbf{q}}) - f(\varepsilon_{\mathbf{k}}))}{\varepsilon_{\mathbf{k}+\mathbf{q}} - \varepsilon_{\mathbf{k}}},$$

where  $f(\varepsilon_{\mathbf{k}})$  represents the Fermi-Dirac distribution with energy  $\varepsilon_{\mathbf{k}}$  (Details in Supplementary Note 2). After solving the equation, we obtain the modified Coulomb potential rising from the carrier screening in reciprocal space:

$$\varphi(\mathbf{q}) = \frac{e}{q(2\varepsilon + q\alpha_{total}^{2D}) - e^2 \chi_{carrier}(\mathbf{q})} \quad (5)$$

The electron screening term emerges separately in the denominator, screening the original 2D

$$\text{Coulomb potential } (\varphi(\mathbf{q}) = \frac{e}{q(2\varepsilon + q\alpha_{total}^{2D})}).$$

### Dipole screening:

Unlike charge carriers, electric dipoles ( $p = Qd$ ) are charge-neutral as a whole but with a finite charge-separated vector. Intuitively, dipole screening can contribute to the screening electrostatic potential via dipole shift and reorientation (Fig.2b). It is usually much weaker than carrier screening and therefore, is conventionally ignored. However, its contribution could be significant in certain scenarios, particularly when considering a moderate dipole

density at 2D system. One example is the small polar molecules in solvents, where the dipole screening dominates the electrostatic interaction<sup>39-41</sup>.

Analogous to charge carrier screening, we calculate the bound charge density due to the surrounding dipoles or excitons. The induced dipole density is obtained using a similar procedure in the previous section.

$$n_{dipole}^{ind}(\boldsymbol{\rho}, t) = e \sum_{\theta} f(\theta) \int_{-\infty}^{+\infty} dt' d^2 \boldsymbol{\rho}' \chi_{dipole}(\boldsymbol{\rho} - \boldsymbol{\rho}'; t - t') \varphi_{\theta}^{ext}(\boldsymbol{\rho}', t') \quad (6)$$

Here,  $\theta$  represents the angle between relative distance  $\boldsymbol{\rho}'$  and dipole orientation  $\mathbf{d}$ ,  $f(\theta)$  is the ratio parameter for different dipole orientation. The potential energy between the external point charge located at origin and dipole at position  $\boldsymbol{\rho}'$  and time  $t'$  with in-plane orientation  $\theta$  is given by  $e\varphi_{\theta}^{ext}(\boldsymbol{\rho}', t') = -e\varphi^{ext}(\boldsymbol{\rho}' - \frac{\mathbf{d}_{\theta}}{2}) + e\varphi^{ext}(\boldsymbol{\rho}' + \frac{\mathbf{d}_{\theta}}{2})$ .

Assuming a highly randomized dipole system ( $f(\theta) = cons.$ ) in a semiclassical way, we can write the induced charge density as:

$$\varrho(\boldsymbol{\rho}, z = 0) = e \sum_{\theta} \left( n_{dipole}^{ind} \left( \boldsymbol{\rho} - \frac{\mathbf{d}_{\theta}}{2}, z = 0 \right) \delta(z) - n_{dipole}^{ind} \left( \boldsymbol{\rho} + \frac{\mathbf{d}_{\theta}}{2}, z = 0 \right) \delta(z) \right) \quad (7)$$

By solving the FT of the Poisson's equation (details in SI), we can obtain the modified Coulomb potential due to dipole or exciton screening in reciprocal space:

$$\varphi(\mathbf{q}, z = 0) = \frac{e}{q(2\varepsilon + q\alpha_{total}^{2D}) - 2e^2\chi_{dipole}(\mathbf{q})(1 - J_0(qd))} \quad (8)$$

where  $\chi_{dipole}(\mathbf{q}) = \frac{1}{S} \sum_k \frac{(f(\epsilon_{k+q}) - f(\epsilon_k))}{\epsilon_{k+q} - \epsilon_k}$ ,  $J_0$  is the zeroth order Bessel function. Note that

$2(1 - J_0(qd)) = \sum_{\theta} 4\sin^2\left(\mathbf{q} \cdot \frac{\mathbf{d}_{\theta}}{2}\right)$ , which comes from the FT of the bound charge density for electric dipole.

	2D	3D
No screening	$\frac{e}{q(2\varepsilon + \alpha_{2D}q)}$	$\frac{e}{\varepsilon q^2}$
Carrier screening	$\frac{e}{q(2\varepsilon + q\alpha_{2D}) - e^2\chi(q)}$	$\frac{e}{\varepsilon q^2 - e^2\chi(q)}$
Dipole screening	$\frac{e}{q(2\varepsilon + q\alpha_{2D}) - 2e^2\chi(q)(1 - J_0(qd))}$	$\frac{e}{\varepsilon q^2 - 2e^2\chi(q)(1 - J_0(qd))}$

Table I: Coulomb potential in 2D and 3D systems without screening, with carrier screening and dipole screening, respectively. The blue region shows the existing formula and the orange region shows our derived results. \*A more detailed calculation of dipole screening is presented in Supplementary Information (SI).

The screened potential in 3D system is calculated analogously and the results are summarized in Table I. The construction of  $\chi_{carrier}(\mathbf{q})$  or  $\chi_{dipole}(\mathbf{q})$  indicates it remain radially

symmetric since the homogeneous particles including charge carrier or charge-neutral dipoles does not break the radial symmetry in 2D plane. When considering both the charge carrier and dipole screening effect simultaneously and ignoring interactions between the carriers and dipoles, one could write a more general modified Coulomb potential as

$$\varphi(\mathbf{q}) = \frac{e}{q(2\varepsilon + q\alpha_{total}^{2D}) - e^2\chi_{carrier}(q) - 2e^2\chi_{dipole}(q)(1 - J_0(qd))} \quad (9)$$

Note that  $\chi_{carrier}(q)$  and  $\chi_{dipole}(q)$  share the similar formula of since the two particle Green's function is applicable for both fermions (carriers) and bosons (dipoles). (details in SI).

### Discussion of the modified Coulomb potential:

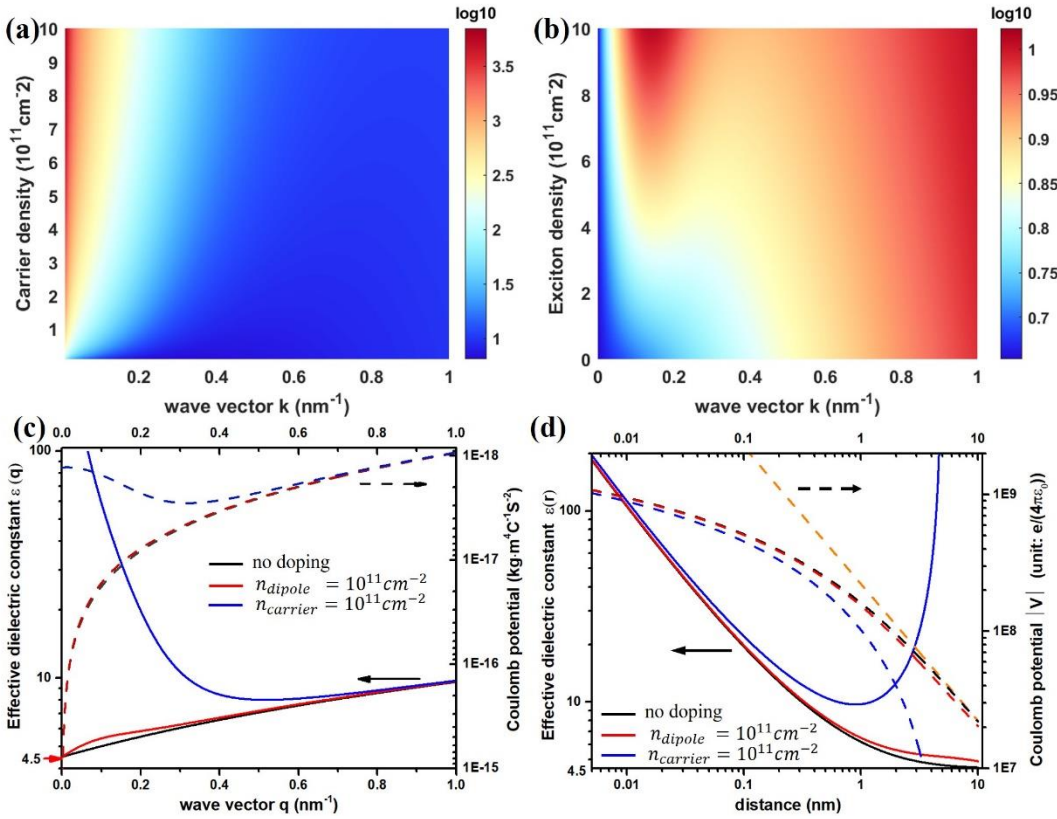


Figure 3: 2D-map of effective dielectric constant as functions of wave vector, carrier density (a) and dipole density (b). (c) Typical screened  $q$ -dependent effective dielectric constant (solid line) and Coulomb potential (dashed line) at  $n_{dipole} = 10^{11} \text{cm}^{-2}$  (red) and  $n_{carrier} =$

$10^{11} \text{cm}^{-2}$  (blue), in comparison to the 2D Coulomb potential  $\varphi(\mathbf{q}) = \frac{e}{q(2\varepsilon + q\alpha_{2D})}$  (black). (d)

Typical screened  $r$ -dependent effective dielectric constant (solid line) and Coulomb potential (dashed line) at  $n_{exciton} = 10^{11} \text{cm}^{-2}$  (red) and  $n_{carrier} = 10^{11} \text{cm}^{-2}$  (blue), in comparison

to the 2D Rytova-Keldysh potential  $V_{2D}(\mathbf{r}, z=0) = \frac{e^2}{8\varepsilon_0 r_0} \left[ H_0\left(\frac{\varepsilon_r r}{r_0}\right) - Y_0\left(\frac{\varepsilon_r r}{r_0}\right) \right]$  (black) and

$V_{3D}(\mathbf{r}) = \frac{e}{4\pi\kappa\varepsilon_0 r}$  (orange).

In 3D system the macroscopic screening effect from the material itself could be simply described by an effective dielectric constant ( $\epsilon_r$ ) in reciprocal space ( $\varphi^{3D}(\mathbf{r}) = \frac{-e}{4\pi\epsilon_r\epsilon_0} \frac{1}{r}$ ;  $\varphi^{3D}(\mathbf{q}) = \frac{-e}{\epsilon_r\epsilon_0} \frac{1}{q}$ ). While in 2D system, it becomes complicated. The highly nonlocal effective dielectric constant is intrinsically  $q$ -dependent and defined as  $\epsilon_{2D}(\mathbf{q}) = \epsilon_r + \frac{\alpha_{2D}q}{2\epsilon_0}$ . Hence, the effective dielectric constant in modified 2D Coulomb potential owing to the carrier and dipole screening effects are defined analogously as  $\epsilon_{carrier}^{2D,eff} = \epsilon_r + \frac{q\alpha_{2D}}{2\epsilon_0} - \frac{e^2\chi(q)}{2q\epsilon_0}$  and  $\epsilon_{dipole}^{2D,eff} = \epsilon_r + \frac{q\alpha_{2D}}{2\epsilon_0} - \frac{2e^2\chi(q)(1-J_0(qd))}{2q\epsilon_0}$ . It is noted that the modified Coulomb potential taking dipole screening into account depends on not only the doping density ( $n$ ), but also dipole size ( $d$ ). In the following calculations, the dipole size is set to be 1.1nm as an practical example to evaluate the modified Coulomb potentials owing to carrier and dipole densities. Fig.3(a) and (b) show the 2D map of  $q$ -dependent effective dielectric constant as functions of carrier and dipole density respectively. Fig.3(c) and Fig.3(d) summarize the effective dielectric constant and the effective Coulomb potentials in reciprocal space as functions of scattering wave vector  $q$  and real spatial distance  $r$  at a typical carrier density ( $10^{11}cm^{-2}$ ) and a dipole density ( $10^{11}cm^{-2}$ ) for comparison. The effective dielectric constant increases with the elevating free carrier (Fig.3a) or dipole density (Fig.3b), indicating that 2D Coulomb potential is strongly influenced by the presence of carriers and dipoles. Besides, the screening effect not only reduces the strength of the Coulomb potential as it does in 3D case, but also results in a significant modification of the potential shape, demonstrating the importance of both carrier and dipole screening effects in 2D materials. The sophisticated behaviours of screened Coulomb potential owing to carrier and dipole density provides possibilities of applications with Coulomb potential engineering.

*Long wavelength approximation ( $q \rightarrow 0$ ):*

For carrier screening, the  $\epsilon_{carrier}^{2D,eff}$  displays a singularity at  $q = 0$  (blue solid line) while the effective Coulomb potential remains a finite value at  $q = 0$  correspondingly, which is similar to the behaviour of Thomas Fermi screening effect in 3D case ( $\epsilon_{carrier}^{3D,eff} = \frac{\epsilon_r\epsilon_0q^2 - e^2\chi(q)}{\epsilon_0q^2}$ ). The main reason for this interesting behaviour is that under the approximation of long wavelength limits,  $\chi(q) = -\partial n/\partial\mu$  is independent on wave vector  $q$  (red ball in FigS.4). In contrast to the carrier screening effect, the screened Coulomb potential (red dashed line in Fig.3c) accounting for dipole screening displays an opposite behaviour. It shows a surprisingly similar tendency to the vacuum 2D Coulomb potential (black dashed line), both diverging at  $q = 0$ . When comparing the effective dielectric constant of dipole screening ( $\epsilon_{dipole}^{2D,eff}$ , red solid line in Fig.3c) to that with zero doping ( $\epsilon_{2D}$ , black solid line in Fig.3c), the exciton screening effect is found to be significant at the range  $q = 0 \sim 0.4nm^{-1}$ , corresponding to the

set of our dipole size ( $d = 1.1\text{nm}$ ).

*Short wavelength and low doping density approximation ( $q \gg k$ ):*

Under this approximation,  $\chi(q)$  can be approximated as  $2nm/\hbar^2 q^2$ , which is dependent on  $q$  as illustrated in FigS.4. It approaches to 0 as  $q$  increases, implying that the screened Coulomb potentials rising from both carrier (blue dashed line) and dipole (red dashed line) exhibit an asymptotical behaviour towards the unscreened 2D Coulomb potential (black dashed line) as the Fig.3c shows.

*Screened Potential in real space:*

The behaviour of screened potentials in real space is similar to that in  $k$ -space. Due to the charge-neutral nature of excitons/dipoles, the screening effect is much weaker compared to charge carrier screening in real space. As a result, the modified Coulomb potential owing to dipole screening changes little, particularly at small relative distances. Notably, the effective dielectric constant as a function of carrier density is non-monotonic, decreasing initially and then increasing. The initial decrease is due to the dielectric movement in the limited 2D plane in the Rytova-Keldysh form, while the increase is similar to the carrier screening effect in the 3D case, as described by the Thomas-Fermi potential ( $V_{3D}^{carrier}(\mathbf{r}) = \frac{e}{4\pi\kappa\epsilon_0 r} e^{-\frac{r}{r_0}}$ ), where the

$r$ -dependent effective dielectric constant shows an exponential increase ( $\epsilon(r) = \kappa e^{\frac{r}{r_0}}$ ).

Furthermore, the similar increase in the effective dielectric constant at large relative distances in the 2D case indicates the short-range and localized nature of the modified Coulomb potential due to carrier screening.

### **Application of the modified Coulomb potential:**

Exciton is a bound quasiparticle consisting of an electron and a hole with a characteristic separation, Bohr radius. Unlike regular dipole, ground-state exciton does not possess a permanent dipole moment in nature owing to the centrosymmetric relative motion described as the  $s$ -type envelope function. Nevertheless, excitons can be approximated as the composition of instantaneous dipoles with complete orientations or in other words, the statistical average of homogeneous dipoles with different orientations, as depicted as the inset of Fig.4a. In this simple approximation, we do not distinguish the screening effect between highly random distributed dipoles and excitons in the following text. Thanks to the large binding energy of exciton in 2D material, excitons are stable even at room temperature and the exciton systems provide a controlled path to track dipole screened Coulomb potential as a function of exciton density in 2D case.

*Estimation of exciton binding energy variation as a function of exciton density*



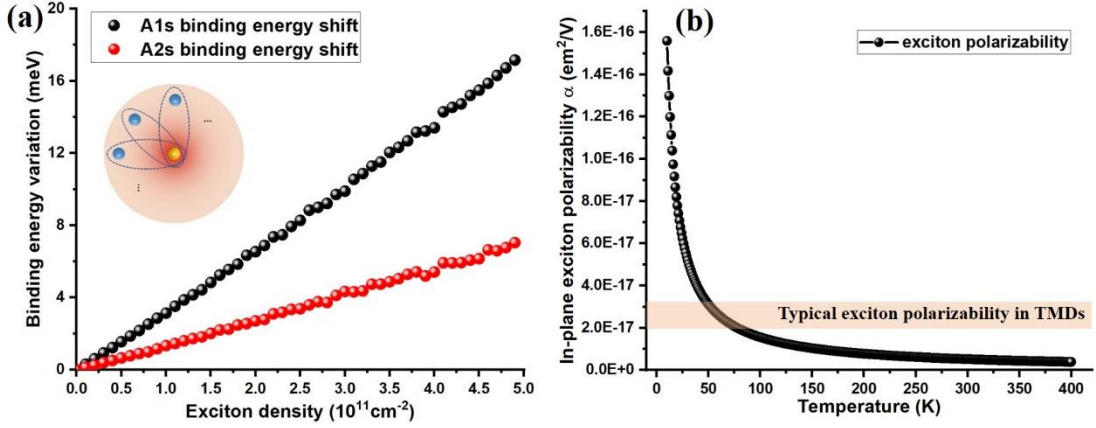


Figure 4: (a) Binding energy shifts of  $1s$  state and  $2s$  states of excitons in monolayer TMD due to the exciton screening effect as a function of exciton density. (b) Temperature dependent exciton polarizability with effective dielectric constant ( $\epsilon_r = 4.5$ ), the orange region shows the typical exciton polarizability ( $\sim 2.5 \times 10^{-17} \text{ em}^2/\text{V}$ ) in monolayer TMDs.

From Fig.3c, the potential modification is mainly located at the range of  $0 \sim 0.4 \text{ nm}^{-1}$ . Given that the effective Bohr radius of ground-state excitons in monolayer TMDs is  $\sim 1 \text{ nm}$ , exactly in this range, the screening effect from exciton population can be significant. Using the dipole screening formula derived in Table I, one can evaluate the change of Coulomb potential via a perturbative term to the initial Coulomb potential under low or medium exciton density. Specifically, the modification in Coulomb potential between exciton-populated and zero-

exciton systems  $\Delta V(q)$  can be approximated as  $\Delta V(q) \approx \frac{2e^3 \chi(q)(1 - J_0(qd))}{q^2(2\epsilon + q\alpha_{2D})^2}$ . This allows us to

calculate the exciton binding energy variation of different Rydberg series excitons using perturbation theory, expressed as:

$$\langle \varphi_{ns}(\mathbf{r}) | V(\mathbf{r}) | \varphi_{ns}(\mathbf{r}) \rangle = \frac{1}{(2\pi)^4} \iint \varphi_{ns}^*(\mathbf{k}_1) \varphi_{ns}(\mathbf{k}_2) \Delta V(\mathbf{k}_1 - \mathbf{k}_2) d\mathbf{k}_1 d\mathbf{k}_2 \quad (10)$$

To perform this calculation, we choose the Rydberg exciton wave function from 2D Hydrogen atom model:  $\psi_{1s}(\mathbf{k}) = 2\sqrt{2\pi} \frac{a_{B,1s}}{[1 + a_{B,1s}^2 k^2]^{3/2}}$  and  $\psi_{2s}(\mathbf{k}) = 2\sqrt{6\pi} \frac{a_{B,2s}}{[1 + a_{B,2s}^2 k^2]^{3/2}} \frac{a_{B,2s}^2 k^2 - 1}{a_{B,2s}^2 k^2 + 1}$ . It is noted that both the ground state ( $1s$ ) and the first excited state ( $2s$ ) exciton wave function of monolayer TMDs are mainly located at the range  $0 \sim 2 \text{ nm}^{-1}$ , which implies the modified Coulomb potential due to exciton screening can effectively tune the exciton binding energy as Fig.3c indicates. We perform a numerical calculation using Monte Carlo method and the results are summarized in Fig.4(b). The binding energies of  $1s$  and  $2s$  excitons increase nearly linearly at the low and medium exciton density regime ( $10^{10} \sim 10^{12} \text{ cm}^{-2}$ ), in accordance with the previous experimental reports.<sup>37</sup> The calculated binding energy shift is slightly overestimated compared to the experiments results, which may be due to the difference between the actual wave function in 2D materials and the wave function of 2D Hydrogen atom model chosen for our numerical calculation.

*Estimation of exciton polarizability in 2D materials:*

Assuming excitons as a rigid object with a modest and uniform polarizability ( $\alpha_{2D}^{ex}$ ) and neglecting their thermal distribution, the modified Coulomb potential takes the form of :

$$\varphi(\mathbf{q}, z = 0) = \frac{e}{q(2\varepsilon_0 + \alpha_{2D}q) + \alpha_{2D}^{ex}nq^2},$$

which means the exciton screened part ( $\alpha_{2D}^{ex}nq^2$ ) is linearly dependent on the exciton density  $n$  in a classical way. On the other hand, under long wavelength approximation ( $q \rightarrow 0$ ), the screened Coulomb potential due to free excitons

$$(eq.8) \text{ can simplify to } \varphi(q) = \frac{e}{q(2\varepsilon_0 + \alpha_{2D}q) + nq^2e^2d^2/2k_B T},$$

where  $n, k_B, T$  are the exciton density, Boltzmann constant and temperature respectively. Comparing these two modified Coulomb potentials, one can conclude that the exciton polarizability is a function of the effective exciton Bohr radius ( $d$ ) and effective exciton temperature, in a simplified formula of

$$\alpha_{2D}^{ex} = \frac{e^2 d^2}{2k_B T}.$$

With the increasing Bohr radius, the exciton polarizability enlarges appropriately since it makes more contribution to polarization per dipole. On the other hand, as temperature increases, disorder sets in, leading to a decrease in exciton polarizability. Taking the dielectric properties into consideration ( $\varepsilon_r = 4.5$ ), the temperature dependent exciton polarizability is plotted in Fig.4b. The typical exciton polarizability in monolayer TMDs are measured to be around  $2.5 \times 10^{17} em^2/V$  using in-plane Stark effect<sup>42-45</sup> or density dependent photoluminescence measurement at 10K, which is a little bit smaller than the theoretical estimation ( $\sim 10^{16} em^2/V$ ). This overestimation may result from that the effective exciton temperature is usually several tens of Kelvin than the lattice temperature (10K) at non-resonant excitation.<sup>46</sup>

### Summary:

In this letter, we present our effective model of the Coulomb potential incorporating screening effect from charged carrier and charge-neutral exciton/dipole in 2D systems. The model elucidates the 2D Coulomb potential modification by charge carrier and exciton population. In conclusion, the modified Coulomb potentials offer a simple and direct way to evaluate the strength of the Coulomb interactions and a design tool for Coulomb potential engineering in 2D systems.

### Acknowledgments

The work was supported by the National Key R&D Program of China (2020YFA0309600), Guangdong-Hong Kong Joint Laboratory of Quantum Matter and the University Grants Committees/Research Grants Council of Hong Kong SAR (AoE/P-701/20, 17300520). The authors thank Prof. Wang Yao for fruitful discussion.

1. Chernikov, A.; Berkelbach, T. C.; Hill, H. M.; Rigosi, A.; Li, Y.; Aslan, B.; Reichman, D. R.; Hybertsen, M. S.; Heinz, T. F., Exciton binding energy and nonhydrogenic Rydberg series in monolayer WS<sub>2</sub>. *Physical review letters* **2014**, *113* (7), 076802.
2. Cudazzo, P.; Tokatly, I. V.; Rubio, A., Dielectric screening in two-dimensional insulators: Implications for excitonic and impurity states in graphane. *Physical Review B* **2011**, *84* (8), 085406.
3. Zhu, B.; Chen, X.; Cui, X., Exciton binding energy of monolayer WS<sub>2</sub>. *Scientific reports* **2015**, *5* (1), 1-5.
4. Ye, Z.; Cao, T.; O'Brien, K.; Zhu, H.; Yin, X.; Wang, Y.; Louie, S. G.; Zhang, X., Probing excitonic dark states in single-layer tungsten disulphide. *Nature* **2014**, *513* (7517), 214-218.
5. Zhang, C.; Johnson, A.; Hsu, C.-L.; Li, L.-J.; Shih, C.-K., Direct imaging of band profile in single layer MoS<sub>2</sub> on graphite: quasiparticle energy gap, metallic edge states, and edge band bending. *Nano letters* **2014**, *14* (5), 2443-2447.
6. Ugeda, M. M.; Bradley, A. J.; Shi, S.-F.; Da Jornada, F. H.; Zhang, Y.; Qiu, D. Y.; Ruan, W.; Mo, S.-K.; Hussain, Z.; Shen, Z.-X., Giant bandgap renormalization and excitonic effects in a monolayer transition metal dichalcogenide semiconductor. *Nature materials* **2014**, *13* (12), 1091-1095.
7. Mak, K. F.; Lee, C.; Hone, J.; Shan, J.; Heinz, T. F., Atomically thin MoS<sub>2</sub>: a new direct-gap semiconductor. *Physical review letters* **2010**, *105* (13), 136805.
8. Jin, C.; Regan, E. C.; Yan, A.; Iqbal Bakti Utama, M.; Wang, D.; Zhao, S.; Qin, Y.; Yang, S.; Zheng, Z.; Shi, S., Observation of moiré excitons in WSe<sub>2</sub>/WS<sub>2</sub> heterostructure superlattices. *Nature* **2019**, *567* (7746), 76-80.
9. Tran, K.; Moody, G.; Wu, F.; Lu, X.; Choi, J.; Kim, K.; Rai, A.; Sanchez, D. A.; Quan, J.; Singh, A., Evidence for moiré excitons in van der Waals heterostructures. *Nature* **2019**, *567* (7746), 71-75.
10. Seyler, K. L.; Rivera, P.; Yu, H.; Wilson, N. P.; Ray, E. L.; Mandrus, D. G.; Yan, J.; Yao, W.; Xu, X., Signatures of moiré-trapped valley excitons in MoSe<sub>2</sub>/WSe<sub>2</sub> heterobilayers. *Nature* **2019**, *567* (7746), 66-70.
11. Navarro-Moratalla, E.; Island, J. O.; Manas-Valero, S.; Pinilla-Cienfuegos, E.; Castellanos-Gomez, A.; Quereda, J.; Rubio-Bollinger, G.; Chirolli, L.; Silva-Guillén, J. A.; Agraït, N., Enhanced superconductivity in atomically thin TaS<sub>2</sub>. *Nature communications* **2016**, *7* (1), 11043.
12. Zhou, J.; Liu, F.; Lin, J.; Huang, X.; Xia, J.; Zhang, B.; Zeng, Q.; Wang, H.; Zhu, C.; Niu, L., Large-area and high-quality 2D transition metal telluride. *Advanced Materials* **2017**, *29* (3), 1603471.
13. Xu, Y.; Liu, S.; Rhodes, D. A.; Watanabe, K.; Taniguchi, T.; Hone, J.; Elser, V.; Mak, K. F.; Shan, J., Correlated insulating states at fractional fillings of moiré superlattices. *Nature* **2020**, *587* (7833), 214-218.
14. Tang, Y.; Li, L.; Li, T.; Xu, Y.; Liu, S.; Barmak, K.; Watanabe, K.; Taniguchi, T.; MacDonald, A. H.; Shan, J., Simulation of Hubbard model physics in WSe<sub>2</sub>/WS<sub>2</sub> moiré superlattices. *Nature* **2020**, *579* (7799), 353-358.
15. Bai, Y.; Liu, S.; Guo, Y.; Pack, J.; Wang, J.; Dean, C. R.; Hone, J.; Zhu, X.-Y., Evidence for Exciton Crystals in a 2D Semiconductor Heterotrilyer. *arXiv preprint arXiv:2207.09601* **2022**.
16. Qiu, D. Y.; Da Jornada, F. H.; Louie, S. G., Screening and many-body effects in two-dimensional crystals: Monolayer MoS<sub>2</sub>. *Physical Review B* **2016**, *93* (23), 235435.
17. Hüser, F.; Olsen, T.; Thygesen, K. S., How dielectric screening in two-dimensional crystals

- affects the convergence of excited-state calculations: Monolayer MoS<sub>2</sub>. *Physical Review B* **2013**, *88* (24), 245309.
18. Noori, K.; Cheng, N. L. Q.; Xuan, F.; Quek, S. Y., Dielectric screening by 2D substrates. *2D Materials* **2019**, *6* (3), 035036.
  19. Keldysh, L., Coulomb interaction in thin semiconductor and semimetal films. *Soviet Journal of Experimental and Theoretical Physics Letters* **1979**, *29*, 658.
  20. Ashcroft, N. W.; Mermin, N. D., *Solid state physics*. Cengage Learning: 2022.
  21. Ross, J. S.; Wu, S.; Yu, H.; Ghimire, N. J.; Jones, A. M.; Aivazian, G.; Yan, J.; Mandrus, D. G.; Xiao, D.; Yao, W., Electrical control of neutral and charged excitons in a monolayer semiconductor. *Nature communications* **2013**, *4* (1), 1474.
  22. Liu, E.; van Baren, J.; Liang, C.-T.; Taniguchi, T.; Watanabe, K.; Gabor, N. M.; Chang, Y.-C.; Lui, C. H., Multipath optical recombination of intervalley dark excitons and trions in monolayer WSe<sub>2</sub>. *Physical Review Letters* **2020**, *124* (19), 196802.
  23. Liu, E.; van Baren, J.; Lu, Z.; Taniguchi, T.; Watanabe, K.; Smirnov, D.; Chang, Y.-C.; Lui, C. H., Exciton-polaron Rydberg states in monolayer MoSe<sub>2</sub> and WSe<sub>2</sub>. *Nature communications* **2021**, *12* (1), 6131.
  24. Xiao, K.; Yan, T.; Liu, Q.; Yang, S.; Kan, C.; Duan, R.; Liu, Z.; Cui, X., Many-body effect on optical properties of monolayer molybdenum diselenide. *The Journal of Physical Chemistry Letters* **2021**, *12* (10), 2555-2561.
  25. He, M.; Rivera, P.; Van Tuan, D.; Wilson, N. P.; Yang, M.; Taniguchi, T.; Watanabe, K.; Yan, J.; Mandrus, D. G.; Yu, H., Valley phonons and exciton complexes in a monolayer semiconductor. *Nature communications* **2020**, *11* (1), 618.
  26. Sidler, M.; Back, P.; Cotlet, O.; Srivastava, A.; Fink, T.; Kroner, M.; Demler, E.; Imamoglu, A., Fermi polaron-polaritons in charge-tunable atomically thin semiconductors. *Nature Physics* **2017**, *13* (3), 255-261.
  27. Mak, K. F.; He, K.; Lee, C.; Lee, G. H.; Hone, J.; Heinz, T. F.; Shan, J., Tightly bound trions in monolayer MoS<sub>2</sub>. *Nature materials* **2013**, *12* (3), 207-211.
  28. Cao, Y.; Fatemi, V.; Fang, S.; Watanabe, K.; Taniguchi, T.; Kaxiras, E.; Jarillo-Herrero, P., Unconventional superconductivity in magic-angle graphene superlattices. *Nature* **2018**, *556* (7699), 43-50.
  29. Parendo, K. A.; Tan, K. S. B.; Bhattacharya, A.; Eblen-Zayas, M.; Staley, N.; Goldman, A., Electrostatic tuning of the superconductor-insulator transition in two dimensions. *Physical review letters* **2005**, *94* (19), 197004.
  30. Ataei, S. S.; Sadeghi, A., Competitive screening and band gap renormalization in n-type monolayer transition metal dichalcogenides. *Physical Review B* **2021**, *104* (15), 155301.
  31. Kang, M.; Jung, S. W.; Shin, W. J.; Sohn, Y.; Ryu, S. H.; Kim, T. K.; Hoesch, M.; Kim, K. S., Holstein polaron in a valley-degenerate two-dimensional semiconductor. *Nature materials* **2018**, *17* (8), 676-680.
  32. Zhang, Z.; Chen, Z.; Bouaziz, M.; Giorgetti, C.; Yi, H.; Avila, J.; Tian, B.; Shukla, A.; Perfetti, L.; Fan, D., Direct observation of band gap renormalization in layered indium selenide. *ACS nano* **2019**, *13* (11), 13486-13491.
  33. Efimkin, D. K.; Laird, E. K.; Levinsen, J.; Parish, M. M.; MacDonald, A. H., Electron-exciton interactions in the exciton-polaron problem. *Physical Review B* **2021**, *103* (7), 075417.
  34. Neidel, C.; Klei, J.; Yang, C.-H.; Rouzée, A.; Vrakking, M.; Klünder, K.; Miranda, M.; Arnold,

- C.; Fordell, T.; L'Huillier, A., Probing time-dependent molecular dipoles on the attosecond time scale. *Physical Review Letters* **2013**, *111* (3), 033001.
35. Gay, J., Screening of excitons in semiconductors. *Physical Review B* **1971**, *4* (8), 2567.
36. Cunningham, P. D.; Hanbicki, A. T.; McCreary, K. M.; Jonker, B. T., Photoinduced bandgap renormalization and exciton binding energy reduction in WS<sub>2</sub>. *ACS nano* **2017**, *11* (12), 12601-12608.
37. Xiao, K.; Yan, T.; Xiao, C.; Fan, F.-r.; Duan, R.; Liu, Z.; Watanabe, K.; Taniguchi, T.; Yao, W.; Cui, X., Exciton-exciton Interaction in Monolayer MoSe<sub>2</sub> from Mutual Screening of Coulomb Binding. *arXiv preprint arXiv:2308.14362* **2023**.
38. Hughes, R. I., Theoretical practice: the Bohm-Pines quartet. *Perspectives on science* **2006**, *14* (4), 457-524.
39. Beglov, D.; Roux, B., An integral equation to describe the solvation of polar molecules in liquid water. *The journal of physical chemistry B* **1997**, *101* (39), 7821-7826.
40. Fedorov, M. V.; Kornyshev, A. A., Ionic liquids at electrified interfaces. *Chemical reviews* **2014**, *114* (5), 2978-3036.
41. Lockhart, D. J.; Kim, P. S., Electrostatic screening of charge and dipole interactions with the helix backbone. *Science* **1993**, *260* (5105), 198-202.
42. Massicotte, M.; Violla, F.; Schmidt, P.; Lundberg, M. B.; Latini, S.; Haastrup, S.; Danovich, M.; Davydovskaya, D.; Watanabe, K.; Taniguchi, T., Dissociation of two-dimensional excitons in monolayer WSe<sub>2</sub>. *Nature communications* **2018**, *9* (1), 1633.
43. Pedersen, T. G., Exciton Stark shift and electroabsorption in monolayer transition-metal dichalcogenides. *Physical Review B* **2016**, *94* (12), 125424.
44. Zhu, B.; Xiao, K.; Yang, S.; Watanabe, K.; Taniguchi, T.; Cui, X., In-Plane Electric Field Induced Orbital Hybridization of Excitonic States In Monolayer WSe<sub>2</sub>. *arXiv preprint arXiv:2302.11373* **2023**.
45. Pu, J.; Matsuki, K.; Chu, L.; Kobayashi, Y.; Sasaki, S.; Miyata, Y.; Eda, G.; Takenobu, T., Exciton polarization and renormalization effect for optical modulation in monolayer semiconductors. *ACS nano* **2019**, *13* (8), 9218-9226.
46. Xiao, K.; Duan, R.; Liu, Z.; Watanabe, K.; Taniguchi, T.; Yao, W.; Cui, X., Hot exciton effect in photoluminescence of monolayer transition metal dichalcogenide. *Natural Sciences* **2023**, *3* (1), e20220035.